Full-Color Emissive MOFs Hot Paper

How to cite: *Angew. Chem. Int. Ed.* **2021**, *60*, 25048 – 25054
International Edition: doi.org/10.1002/anie.202110531
German Edition: doi.org/10.1002/ange.202110531

Tuning and Directing Energy Transfer in the Whole Visible Spectrum through Linker Installation in Metal–Organic Frameworks

Daming Ren[+], Hai-Lun Xia[+], Kang Zhou, Shenjie Wu, Xiao-Yuan Liu, Xiaotai Wang, and Jing Li**

Abstract: *While limited choice of emissive organic linkers with systematic emission tunability presents a great challenge to investigate energy transfer (ET) over the whole visible light range with designable directions, luminescent metal-organic frameworks (LMOFs) may serve as an ideal platform for such study due to their tunable structure and composition. Herein, five Zr_6 cluster-based LMOFs, HIAM-400X (X = 0, 1, 2, 3, 4) are prepared using 2,1,3-benzothiadiazole and its derivative-based tetratopic carboxylic acids as organic linkers. The accessible unsaturated metal sites confer HIAM-400X as a pristine scaffold for linker installation. Six full-color emissive 2,1,3-benzothiadiazole and its derivative-based dicarboxylic acids (L) were successfully installed into HIAM-400X matrix to form HIAM-400X-L, in which the ET can be facilely tuned by controlling its direction, either from the inserted linkers to pristine MOFs or from the pristine MOFs to inserted linkers, and over the whole range of visible light. The combination of the pristine MOFs and the second linkers via linker installation creates a powerful two-dimensional space in tuning the emission via ET in LMOFs.*

Introduction

In the natural photosystem, light absorption and subsequent energy transfer (ET) are the crucial initial steps to converting solar energy to biological energy, in which nature employs well-ordered complexes to achieve highly efficient solar energy utilization.[1,2] To mimic such highly optimized natural ET process, various artificial light-harvesting materials have been developed.[3–10] Among them, organic linker-based luminescent metal-organic frameworks (LMOFs)[11–14] have been developed recently as a useful platform to study ET.[6–10,15] Due to the unique structural tunability and unlimited compositions, the distances and angles between different kinds of organic linkers in the MOF matrixes can be precisely controlled and determined by single-crystal X-ray diffraction methods, which provide multiple ways to tune and study ET. So far, two structural models have been built as depicted in Scheme 1. Model I possesses pillar-layered structures, in which two kinds of organic linkers, one as donor and the other one as acceptor, are incorporated into the MOF matrix with ordered distribution.[16–21] Model II uses mixed-linker strategy to incorporate two linkers into a single crystal structure with disordered distribution.[22–24] While many interesting and important studies have been done based on these two models, most of these studies are limited to two linkers with restrictions on their absorption and emission properties, with very limited capability to tune the ET in the whole visible light range and to control its direction.

Linker installation has been proven to be a useful strategy to insert targeted second linker into the pristine MOFs to confer specific properties or new functions on resultant MOFs.[25–30] It has been utilized to improve MOF performance for various applications such as catalysis,[31,32] sensing[33] and gas sorption[34,35] after first reported in 2015.[25] Accordingly, the third model (Model III) can be developed based on linker installation to investigate the ET between pristine linkers and inserted second linkers (Scheme 1). Under this strategy, three approaches may be used to systematically tune ET with controllable directions over the whole visible spectrum: (a) full-color emissive pristine MOFs with single emissive second linker, (b) single emissive pristine MOF with full-color emissive second linkers, (c) full-color emissive pristine MOFs with full-color emissive second linkers. However, to this date, no work has been reported on achieving tunable ET in the whole visible light range using one of these three approaches. The main challenge lies in synthesizing organic linker-based full-color emissive MOFs or second linkers, and tuning the ET in the whole visible spectrum. We have recently discovered that full-color emissive UiO-68 type MOFs can be prepared using 2,1,3-benzothiadiazole and its derivative-based dicarboxylic acids,[36] which inspires us to extend this strategy to the design of LMOFs with multi-fold tunability using similar organic linkers to systematically control and direct ET process.

[*] D. Ren,[+] Dr. H.-L. Xia,[+] Dr. K. Zhou, S. Wu, Prof. X.-Y. Liu, Prof. X. Wang, Prof. J. Li
Hoffmann Institute of Advanced Materials, Shenzhen Polytechnic
7098 Liuxian Blvd, Nanshan District, Shenzhen, 518055 (People's Republic of China)
E-mail: liuxiaoyuan1989@szpt.edu.cn
Prof. X. Wang
Department of Chemistry, University of Colorado Denver
Campus Box 194, P. O. Box 173364, Denver, Colorado 80217-3364 (USA)
Prof. J. Li
Department of Chemistry and Chemical Biology, Rutgers University
123 Bevier Road, Piscataway, New Jersey 08854 (USA)
E-mail: jingli@rutgers.edu
[+] These authors contributed equally to this work.
Supporting information and the ORCID identification number(s) for the author(s) of this article can be found under: https://doi.org/10.1002/anie.202110531.

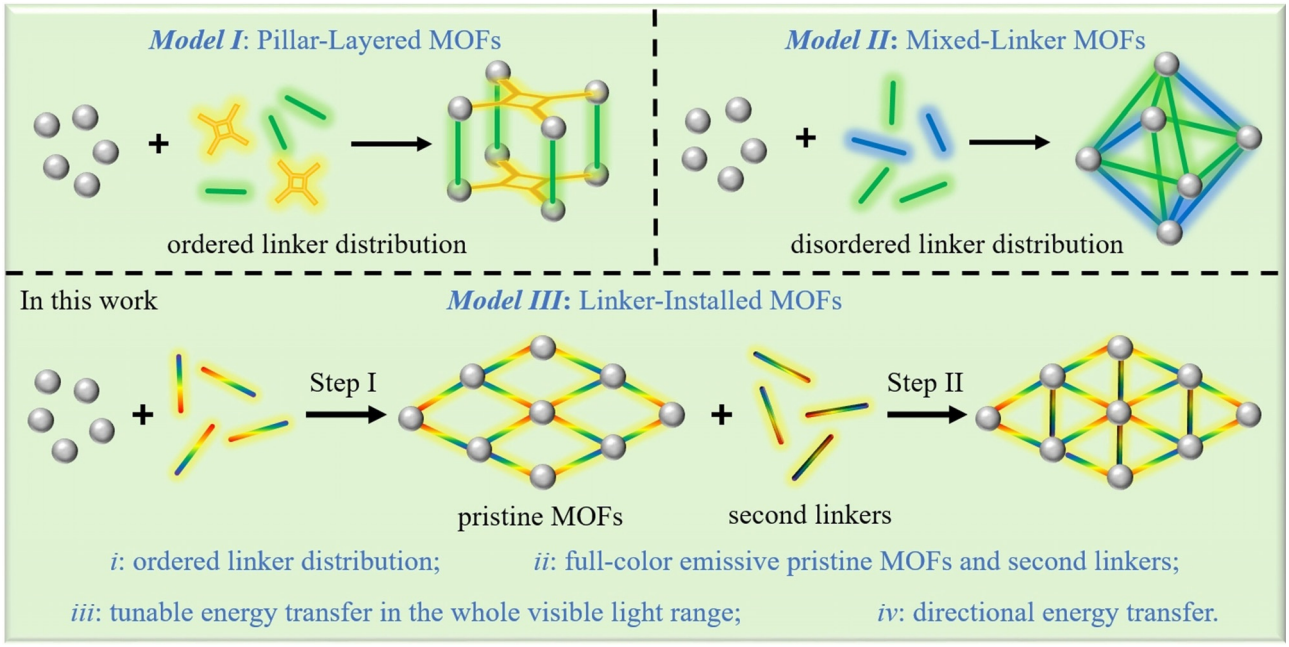

Scheme 1. Schematic diagram illustrating three models of organic linker-based MOFs for energy transfer. Model I: Pillar-layered MOFs with ordered linkers distributions. Model II: Mixed-linker MOFs with disordered linkers distributions. Model III: Linker-installed MOFs with ordered linkers distributions and designable directions for tunable energy transfer over the whole visible light range.

Results and Discussion

Based on the aforementioned considerations, we attempt to realize tunable ET in the whole visible spectrum with controlled directions via linker installation using approach (c) in Model III, which is the combination of approach (a) and (b), namely combination of full-color emissive pristine MOFs and full-color emissive second linkers. For preparing full-color emissive pristine MOFs, we firstly designed and synthesized five tetratopic carboxylate linker via Suzuki reactions and followed hydrolysis under mild conditions as shown in Figure 1 a. These are 5′,5‴′-(5,6-dimethylbenzo[c]-[1,2,5]thiadiazole-4,7-diyl)bis([1,1′:3′,1″-terphenyl]-4,4″-di-carboxylic acid) (DTTC), 5′,5‴′-(benzo[c][1,2,5]thiadiazole-4,7-diyl)bis(([1,1′:3′,1″-terphenyl]-4,4″-dicarboxylic acid)) (BTTC), 5′,5‴′-(benzo[c][1,2,5]selenadiazole-4,7-diyl)-bis(([1,1′:3′,1″-terphenyl]-4,4″-dicarboxylic acid)) (BSTC), 5′,5‴′-(naphtho[2,3-c][1,2,5]thiadiazole-4,9-diyl)-bis(([1,1′:3′,1″-terphenyl]-4,4″-dicarboxylic acid)) (NTTC), and 5′,5‴′-(naphtho[2,3-c][1,2,5]selenadiazole-4,9-diyl)-bis(([1,1′:3′,1″-terphenyl]-4,4″-dicarboxylic acid)) (NSTC). These linkers have similar molecular skeleton with the tetratopic carboxylate ligand used to synthesize NPF-300 and PCN-808, where various second linkers can be inserted into the pristine structures to achieve proposed properties.[28,32] Therefore, we envision that these five linkers could also be employed to prepare MOFs with unsaturated open metal sites available for second linker installation post-synthetically. We first investigated the photoluminescence (PL) behaviors of these linkers in solution. As expected, the emissions from DTTC to NSTC cover the whole visible light range from blue to red (Figure S1), which is similar to what we have observed in linkers with the same Ar core in our previous work.[36] Density functional theory (DFT) was utilized to calculate the molecular orbital energies of the linkers. As depicted in Figure S2, the highest occupied molecular orbital (HOMO) energies gradually increases while the lowest unoccupied molecular orbital (LUMO) energies monotonically decreases from DTTC to NSTC, resulting in a decrease of HOMO–LUMO energy gap, consistent with the observed emission energies and previously reported work.[37,38]

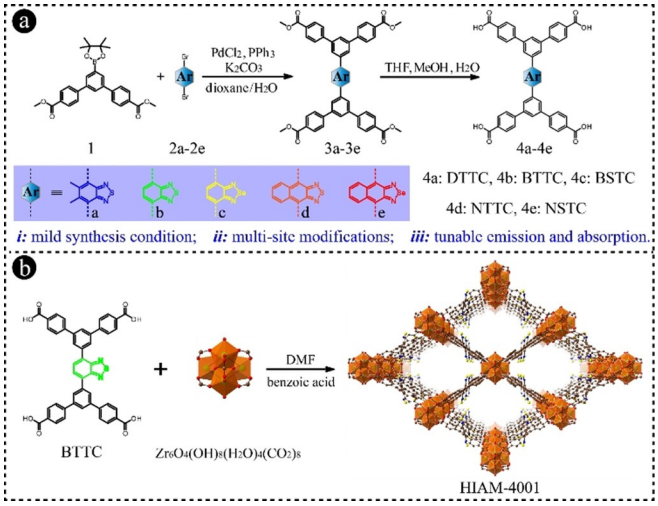

Figure 1. a) The synthetic routes and molecular structures of the five tetratopic carboxylate linkers with tunable absorption and emission energies; b) the synthetic condition and crystal structure of HIAM-4001 viewed along the *c* axis (green Zr; red O; brown C; yellow S; blue N).

A typical synthesis protocol for obtaining single crystals of the proposed MOFs, HIAM-400X (HIAM = Hoffmann Institute of Advanced Materials; 40 = Zirconium; X = 0 for DTTC, X = 1 for BTTC, X = 2 for BSTC, X = 3 for NTTC and X = 4 for NSTC), is schematically shown in Figure 1b: a 5 mL vial containing 23.3 mg $ZrCl_4$, 10.0 mg linkers (BTTC for HIAM-4001), 700 mg benzoic acid and 3 mL N,N-dimethylformamide (DMF) was placed in a preheated oven for 4 days at 120 °C. After cooling to room temperature, colorless (HIAM-4000), light yellow (HIAM-4001), yellow (HIAM-4002), light orange (HIAM-4003) and light red (HIAM-4004) crystals were obtained (Figure 2a and Figure S3). While single crystals of all five HIAM-400X samples were obtained, only the crystal structure of HIAM-4001 (CCDC NO. 2096594)was refined with high quality (Table S1). Therefore, HIAM-4001 was used for the following structural characterization. Single-crystal X-ray diffraction (sc-XRD) measurement at 295 K shows that HIAM-4001 crystallizes in the orthorhombic crystal system with a Cmmm space group and a scu topology, which is the same as NPF-300.[28] As shown in Figure 1b, each Zr_6 cluster connects to eight fully deprotonated BTTC linker and eight terminal H_2O/OH^- groups. Each BTTC is connected to four Zr_6 clusters. Within the structure of HIAM-4001, four types of one-dimensional (1D) open channels are formed, namely, rhombic channels and hexagonal channels along *a* axis, rhombic channels along *b* axis and rhombic channels along *c* axis (Figure 1b and Figure S4).

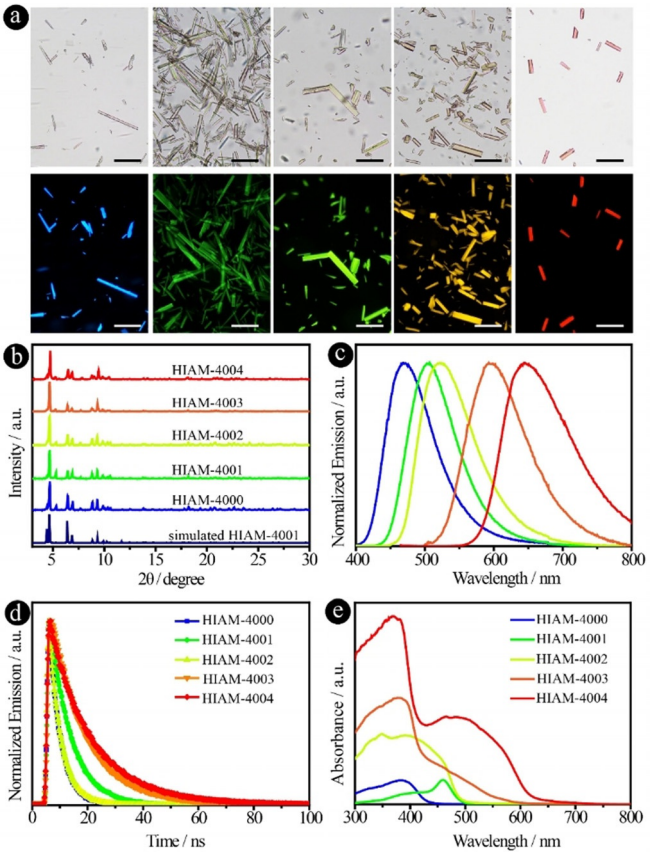

Figure 2. a) The single-crystal images of HIAM-400X under daylight and photoexcitation (365 nm for HIAM-4000, 450 nm for HIAM-4001, HIAM-4002, HIAM-4003 and HIAM-4004; scale bar: 100 μm), b) the PXRD patterns, c) normalized solid-state emission spectra, d) transient PL decay profiles and e) UV-vis absorption spectra of HIAM-4000, HIAM-4001, HIAM-4002, HIAM-4003 and HIAM-4004.

As shown in Figure 2b, the PXRD patterns of the as-synthesized HIAM-400X compounds exhibit an excellent agreement with the simulated patterns of HIAM-4001, confirming their isoreticular nature as well as the phase purity. The solid-state PL spectra and the transient PL decay of HIAM-400X show similar trend as observed for UiO-68 type MOFs with the same Ar core (Figure 2c and d).[36] Tunable emission from blue to red was recorded for HIAM-400X with peak maxima at 470, 505, 522, 595 and 645 nm for HIAM-4000, HIAM-4001, HIAM-4002, HIAM-4003 and HIAM-4004, respectively, which is consistent with the emissive colors of their single-crystals (Figure 2a and c). The corresponding PL quantum yields (PLQYs) of the HIAM-4000 to HIAM-4004 are 21.1%, 44.0%, 28.4%, 17.6% and 7.70% under 365 nm excitation. At 450 nm excitation, the PLQYs are 26.2%, 19.9% and 9.20% for HIAM-4002, HIAM-4003 and HIAM-4004, respectively. The emission of HIAM-400X is linker-based due to the fact that the electronic band gap of zirconium (IV) oxo nodes is much larger than that of organic linkers.[39–41] As a result, no electron or charge transfer will occur between the Zr_6 cluster and linkers, which is further confirmed via the DFT calculation using the fraction of HIAM-4001 as an example (Figure S5). Both HOMO and LUMO of HIAM-4001 resemble those of the BTTC linker without any contribution from Zr metal, which is similar with our previous work.[36] A gradual bathochromic-shift was observed in the UV-vis absorption spectra from HIAM-4000 to HIAM-4004, which is also consistent with their corresponding emission energies (Figure 2e). It should be noted that HIAM-4003 and HIAM-4004 exhibit a much broader light absorption range, which could be used as blue-light excitable phosphors or photocatalysts. All five HIAM-400X compounds show excellent thermal stability with the framework remaining intact up to ≈500 °C (Figure S6). The above results demonstrate that our strategy in using 2,1,3-benzothiadiazole and its derivatives as core for the synthesis of luminescence organic linkers represents an efficient and universal approach, and can be used to design and synthesize MOFs with well tunable structures and porosity in addition to their luminescence. More importantly, the resultant HIAM-400X series, consisting 8-connected $Zr_6O_4(OH)_8(H_2O)_4$ clusters with 8-unsaturated open metal sites, makes an ideal platform for post-synthetic second linker installation by replacing the terminal OH^-/H_2O groups on the clusters.

As depicted in Figure 3a and b, the distance between unsaturated metal sites of two neighboring Zr_6 clusters perpendicular to *a* and *c* axis are 1.24 nm and 1.51 nm, respectively, indicating that two kinds of second linkers with different lengths could be installed into the channels through unsaturated metal centers. The lengths of 2,1,3-benzothiadiazole and its derivative-based dicarboxylic acids (L), i.e., 4,4′-(2H-benzo[d][1,2,3]triazole-4,7-diyl)bis(3-methoxybenzoic acid) (BAMB), 4,4′-(5,6-dimethylbenzo[c][1,2,5]thiadiazole-4,7-diyl)dibenzoic acid (MBTB), 4,4′-(benzo[c]-[1,2,5]thiadiazole-4,7-diyl)bis(3-methoxybenzoic acid)

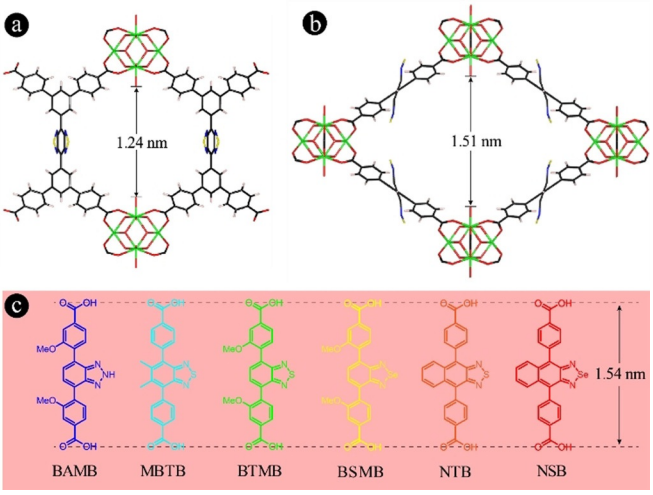

Figure 3. a),b) The crystal structure of HIAM-4001 viewed along the *a* and *c* axis with the distance marked between two Zr_6 cluster for linker installation, c) molecular structures of the six second linkers used in this study.

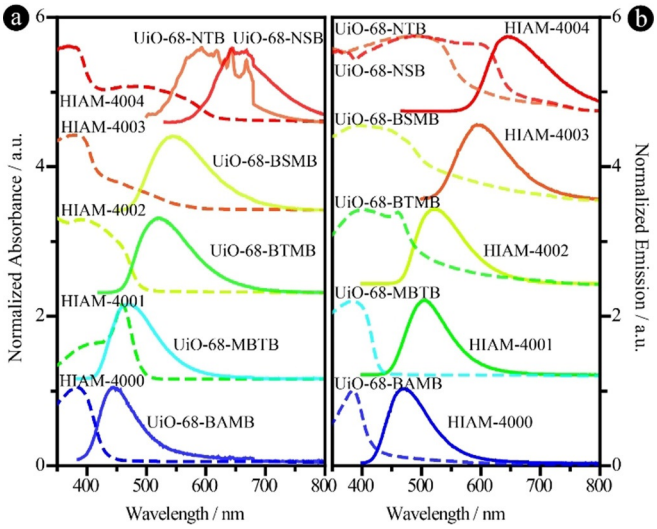

Figure 4. a) The normalized UV-vis absorption spectra (dotted line) of HIAM-4000 (blue line), HIAM-4001 (green line), HIAM-4002 (yellow line), HIAM-4003 (orange line) and HIAM-4004 (red line) and the normalized emission spectra (solid line) of UiO-68-BAMB (blue line), UiO-68-MBTB (cyan line), UiO-68-BTMB (green line), UiO-68-BSMB (yellow line), UiO-68-NTB (orange line) and UiO-68-NSB (red line); b) the normalized UV-vis absorption spectra (dotted line) of UiO-68-BAMB (blue line), UiO-68-MBTB (cyan line), UiO-68-BTMB (green line), UiO-68-BSMB (yellow line), UiO-68-NTB (orange line) and UiO-68-NSB (red line) and the normalized emission spectra (solid line) of HIAM-4000 (blue line), HIAM-4001 (green line), HIAM-4002 (yellow line), HIAM-4003 (orange line) and HIAM-4004 (red line).

(BTMB), 4,4′-(benzo[c][1,2,5]selenadiazole-4,7-diyl)bis(3-methoxybenzoic acid) (BSMB), 4,4′-(naphtho[2,3-c]-[1,2,5]thiadiazole-4,9-diyl)bis(3-methoxybenzoic acid) (NTMB) and 4,4′-(naphtho[2,3-c][1,2,5]selenadiazole-4,9-diyl) bis(3-methoxybenzoic acid) (NSMB), are all around 1.54 nm (Figure 3c), which matches well with the distance of the open pockets along the *c* axis of HIAM-4001. Therefore, it should be feasible to install these linkers into the pristine crystal structures of HIAM-400X to form HIAM-400X-L. In addition, these six second linkers emit a broad range of light from blue to red color (Figure S7), which suggests that tunable ET might be achievable between pristine HIAM-400X and the second linkers once they are inserted into the unsaturated metal sites.

We then first assessed possible energy transfer by comparing the UV-vis absorption and emission spectra of HIAM-400X and the UiO-68-L type MOFs (Figures S8,S9), where L represents the second linker to be inserted in HIAM-400X.[36] This is relevant, as the emission of the UiO-68-L series is ligand centered and the optical behaviors of the ligands (L) are most likely to be very similar in UiO-68-L and in HIAM-400X-L after being inserted in HIAM-400X as the second linkers. As shown in Figure 4a,b, various degrees of overlap between the emission spectra of UiO-68-L (as energy donor) and the UV-vis absorption spectra of HIAM-400X (as energy acceptor), or between the emission spectra of HIAM-400X (as energy donor) and the UV-vis absorption spectra of UiO-68-L (as energy acceptor) were observed. For instance, the emission spectrum of UiO-68-BAMB (as donor) overlaps substantially with the absorption spectra of the HIAM-400X series (as acceptor), indicating that its emission energy can be absorbed by all five HIAM-400X compounds. The absorption spectrum of UiO-68-NSB (as acceptor) almost covers the entire emission spectra of HIAM-400X (as donor), particularly HIAM-4000, -4001 and 4002, demonstrating that the emission energy of these HIAM-400X can be transferred nearly completely to UiO-68-NSB. More importantly, MOFs with absorption and emission spectra located in the middle region of the visible light spectrum can serve efficiently both as an energy donor and acceptor. For example, HIAM-4002 can absorb emission energy from MOFs made of linkers with higher HOMO–LUMO gaps, such as BAMB and MBTB, while donating its emission energy to MOFs made of linkers with lower HOMO–LUMO gaps, such as NTB and NSB. This will enable directed energy transfer to occur from the post-synthetically installed second linkers (e.g. BAMB and MBTB in UiO-68-L) to pristine linkers (e.g. BSTC in HIAM-4002) or from pristine linkers (e.g. BSTC in HIAM-4002) to post-synthetically installed second linkers (e.g. NTB and NSB in UiO-66-L) once the second linkers are installed to HIAM-400X series. Thus, various combinations of the pristine MOFs (HIAM-400X) and the second linkers (Figure 3c) via linker installation will create a powerful two-dimensional (2D) space in tuning the energy transfer within the whole visible light spectrum.

To prove this hypothesis and achieve tunable ET in the whole visible light range, the six second linkers (Figure 3c) were installed into the pristine HIAM-400X via single-crystal to single-crystal transformation. After removal of terminal OH^-/H_2O groups, the unsaturated metal sites perpendicular to the *c* axis in HIAM-400X can be replaced by selected second linkers via incubating single-crystals HIAM-400X in DMF solution containing second linkers. While we succeeded in growing single crystals of several HIAM-400X-L samples and obtained preliminary structure for all of them, the final structure refinement was found very difficult due to their

generally low diffraction, except for HIAM-4001-BTMB (CCDC NO. 2096595), HIAM-4002-BAMB (CCDC NO. 2096596) and HIAM-4003-MBTB (CCDC NO. 2096597) (Table S2–S4). Therefore, the following characterizations are based on HIAM-4002-BAMB due to its high quality (Figure 5a and b, Figure S10 and Table S3). As shown in

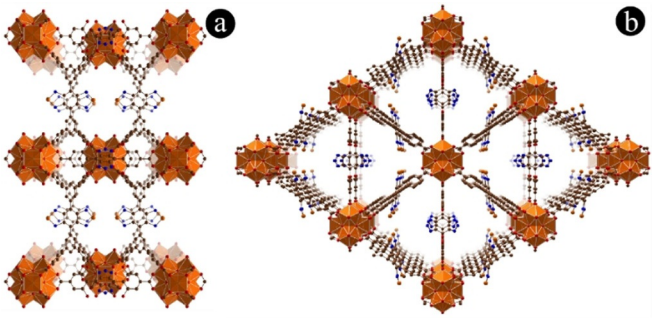

Figure 5. The crystal structure of HIAM-4002-BAMB viewed along the a) *a* axis and b) *c* axis (green Zr; red O; brown C; orange Se; blue N).

Figure 5b, BAMB is inserted into the rhombic channel of HIAM-4002, resulting in two identical trigonal channels in HIAM-4002-BAMB along the *c* axis. As depicted in Figure 6a1–e1, PXRD patterns of as-synthesized thirty HIAM-400X-L compounds show excellent agreement with the simulated PXRD pattern of HIAM-4002-BAMB, indicating the same crystal structure for all of them. The successful linker installation is also confirmed by the changes in the optical absorption spectra after inserting different second linkers with varying light harvesting capacity. As shown in Figure 6a2–e2, the absorption spectra of the HIAM-400X-L series show blue-shift when the light harvesting range of L is narrower than the pristine HIAM-400X, while a red-shift was observed if the light harvesting spectrum of L is boarder than the pristine HIAM-400X.

We then collected solid-state PL spectra, transient PL decay profiles and PLQY of the thirty MOFs to study the ET between pristine HIAM-400X and inserted second linkers (Figure 6, Figure S11 and Table S5). For HIAM-4000-BAMB, HIAM-4000-MBTM, HIAM-4000-BTMB, HIAM-4000-BSMB, HIAM-4000-NTB and HIAM-4000-NSB, as depicted in Figure 6a3 and Figure 7, six emission spectra covering the whole visible light range from blue to red were measured with the peak maxima at 479, 476, 506, 540, 598 and 646 nm, respectively, consistent with the emission energies and color of the corresponding HIAM-4000-L series under daylight and 365 nm excitation (Figure 7a). Compared with the emission peak maxima of HIAM-4000 (470 nm), UiO-68-BAMB (445 nm), UiO-68-MBTB (470 nm), UiO-68-BTMB (520 nm), UiO-68-BSMB (545 nm), UiO-68-NTB (593 nm) and UiO-68-NSB (654 nm), the emission peak of BAMB disappeared in HIAM-4000-BAMB and the emission peak belong to HIAM-4000 disappeared in HIAM-4000-BTMB, HIAM-4000-BSMB, HIAM-4000-NTB and HIAM-4000-NSB. These results demonstrate that the ET is from BAMB to pristine linker in HIAM-4000-BAMB and from the pristine linker to the second linkers in HIAM-4000-BTMB, HIAM-4000-BSMB, HIAM-4000-NTB and HIAM-4000-NSB. Two

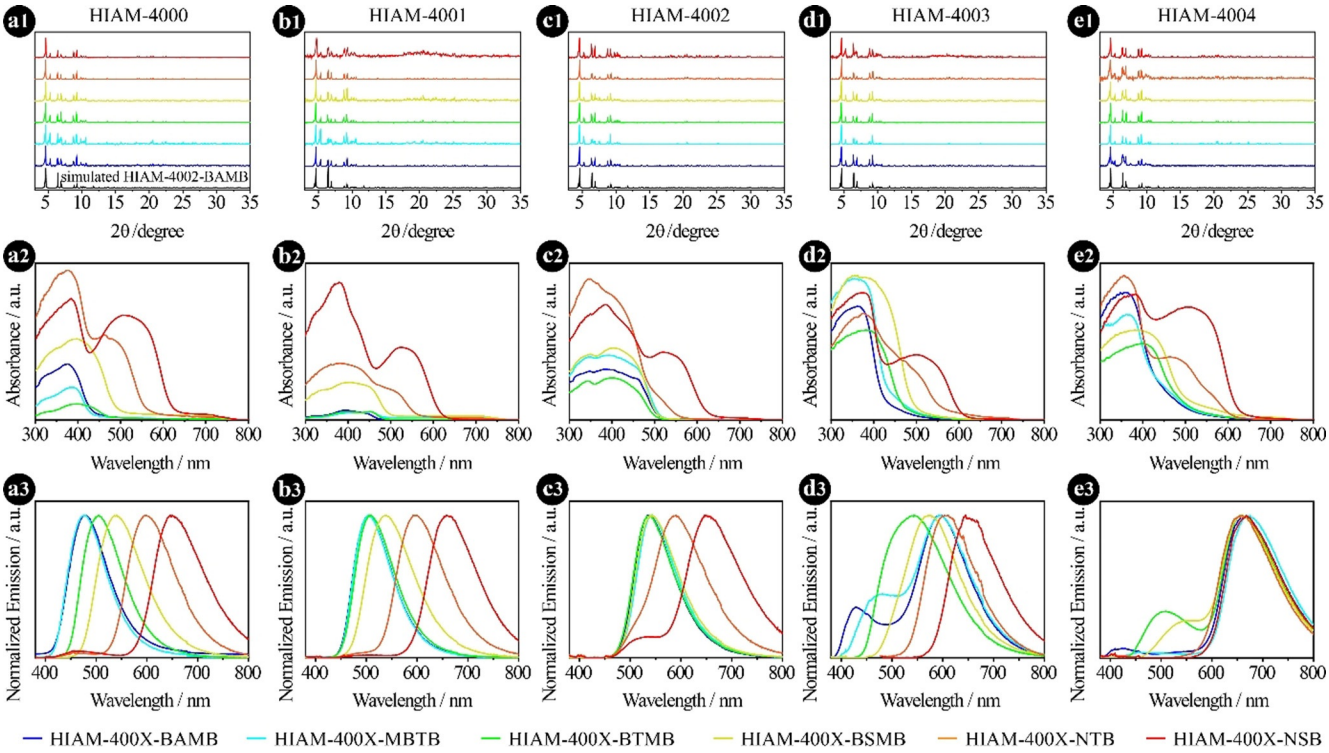

Figure 6. (a1–e1) The PXRD patterns, (a2–e2) the UV-vis absorption and (a3–e3) the solid-state emission spectra of HIAM-400X-BAMB, HIAM-400X-MBTB, HIAM-400X-BTMB, HIAM-400X-BSMB, HIAM-400X-NTB, HIAM-400X-NSB (for a, X=0; for b, X=1; for c, X=2; for d, X=3; for e, X=4) under 365 nm excitation.

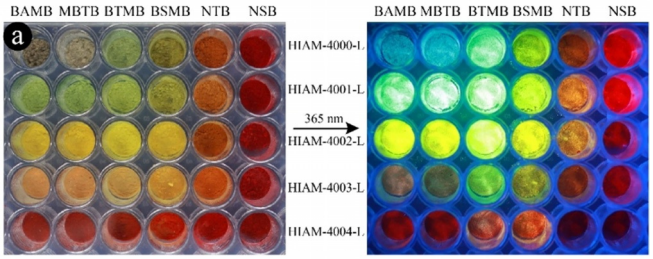

b

	-	BAMB	MBTB	BTMB	BSMB	NTB	NSB
HIAM-4000-L	470	479	476	506	540	598	646
HIAM-4001-L	505	506	503	506	539	599	658
HIAM-4002-L	522	538	542	538	544	590	648
HIAM-4003-L	595	596	593	544	573	609	645
HIAM-4004-L	645	667	675	655	659	657	667

Figure 7. a) The photographs of HIAM-400X-L under daylight and 365 nm excitation, and b) the large emission peak maxima (nm) of HIAM-400X-L under 365 nm excitation. (Columns marked in blue: Energy transfer from second linkers to the pristine MOFs; Columns marked in red: energy transfer from pristine MOFs to the second linkers.)

smaller emission peaks around 460 nm belonging to pristine linker were observed for HIAM-4000-NTB and HIAM-4000-NSB, indicating that ET from pristine linker to NTB and NSB is not less pronounced in these two MOFs. It is also clear that the PLQYs of the HIAM-4000-L group are generally lower than those of the HIAM-4000 series (Table S5), which can be ascribed to the properties of the inserted linkers, suggesting the energy loss during the energy transfer process. The successful linker installation was also confirmed by ^{1}H NMR of digested HIAM-4000-L samples (Figures S12–S17). The molar ratio of MBTB:DTTC in digested HIAM-4000-MBTB is 0.46 according to the ^{1}H NMR spectra, which is close to the theoretical value of 0.5. However, it should be noted that, for HIAM-4000-BAMB, HIAM-4000-BTMB and HIAM-4000-BSMB, the ratio is much higher than 0.5, which could be attributed to the fact that some of linkers may coordinate to the unsaturated metal sites with only one carboxylate, resulting in dangling end.[28,32] While for HIAM-4000-NTB and HIAM-4000-NSB, the ratio is much lower than 0.5 owing to the steric hindrance of naphtho[2,3-c][1,2,5]thiadiazole and naphtho[2,3-c][1,2,5]selenadiazole group.[32]

Similar results were observed for HIAM-4001-L, HIAM-4002-L and HIAM-4004-L (Figure 6b3, c3, e3, Figure 7a and b). When the emission spectra of the second linkers have ample overlap with the absorption spectra of the pristine MOFs, the ET occurs from the second linkers to pristine MOFs and the emission peaks of second linkers will decrease/disappear. When the emission spectra of the pristine MOFs show great overlap with the absorption spectra of the second linkers, the ET happens from the pristine MOFs to the second linkers, resulting in disappeared emission peak belonging to pristine MOFs. It should be noted that the obvious emission peaks originating from the second linkers (BTMB and BSMB) were found for the samples of HIAM-4004-BTMB and HIAM-4004-BSMB, indicating that the ET is insufficient from BTMB and BSMB to NSTC. However, for HIAM-4003-L, the ET process is even more inefficient from the installed linkers to the pristine linkers, especially for BTMB and BSMB (Figure 6d3). As shown in Figure 7b, the emission peaks of HIAM-4003-BTMB and HIAM-4003-BSMB have a red-shift of 24 and 28 nm, respectively, compared with those of UiO-68-BTMB and UiO-68-BSMB, while a blue-shift of 49 and 20 nm were measured compared with the emission peak of HIAM-4003. These results suggest that the emission spectra of HIAM-4003-BTMB and HIAM-4003-BSMB are a combination of the emissions from both the pristine and the inserted linkers. From these results, it is clear that the ET can be realized between the pristine linkers and second linkers with controlled directions in the whole visible light range via linker installation.

Conclusion

In summary, five metal-organic frameworks, HIAM-400X with tunable emission colors from blue to red have been designed and synthesized using 2,1,3-benzothiadiazole and its derivative-based tetratopic carboxylates as organic linkers. The **scu** topology enables the HIAM-400X series an ideal platform for linker installation via the replacement of the terminal OH^-/H_2O groups on the 8-connected $Zr_6O_4(OH)_8(H_2O)_4$ clusters. The combination of five emissive HIAM-400X and six second linkers through linker installation yield thirty HIAM-400X-L structures with systematically tunable and well controlled energy transfer in the whole visible spectrum. The energy transfer can be directed from second linkers to the pristine MOFs or from pristine MOFs to the second linkers. To the best of our knowledge, HIAM-400X-L represents the first series of LMOFs that offer a two-dimensional space for tuning emissions. Such a strategy provides a new model to achieve a high level of directed energy transfer and inspires the rational design of materials for light-harvesting, energy transfer and related applications.

Acknowledgements

The authors gratefully acknowledge the support from Shenzhen Polytechnic. X.-Y. Liu acknowledges the financial support from Guangdong Basic and Applied Basic Research Foundation (2020A1515110420) and Shenzhen Science and Technology Program (RCBS20200714114941230).

Conflict of Interest

The authors declare no conflict of interest.

Keywords: energy transfer · full-color emission · linker installation · metal–organic frameworks (MOFs) · tunable emission

[1] G. D. Scholes, G. R. Fleming, A. Olaya-Castro, R. van Grondelle, *Nat. Chem.* **2011**, *3*, 763 – 774.
[2] J. Barber, P. D. Tran, *J. R. Soc. Interface* **2013**, *10*, 20120984.
[3] D. R. Whang, D. H. Apaydin, *ChemPhotoChem* **2018**, *2*, 148 – 160.
[4] S. M. Baxter, W. E. Jones, E. Danielson, L. Worl, G. Strouse, J. Younathan, T. J. Meyer, *Coord. Chem. Rev.* **1991**, *111*, 47 – 71.
[5] N. Aratani, D. Kim, A. Osuka, *Acc. Chem. Res.* **2009**, *42*, 1922 – 1934.
[6] M. C. So, G. P. Wiederrecht, J. E. Mondloch, J. T. Hupp, O. K. Farha, *Chem. Commun.* **2015**, *51*, 3501 – 3510.
[7] D. E. Williams, N. B. Shustova, *Chem. Eur. J.* **2015**, *21*, 15474 – 15479.
[8] C. R. Martin, P. Kittikhunnatham, G. A. Leith, A. A. Berseneva, K. C. Park, A. B. Greytak, N. B. Shustova, *Nano Res.* **2021**, *14*, 338 – 354.
[9] Z. Wang, C. Wang, *Adv. Mater.* **2021**, *0*, 2005819.
[10] J. Zhu, S. Shaikh, N. J. Mayhall, A. J. Morris, *Elaboration and Applications of Metal-Organic Frameworks*, World Scientific, Singapore, **2018**, pp. 581 – 654.
[11] Y. Cui, Y. Yue, G. Qian, B. Chen, *Chem. Rev.* **2012**, *112*, 1126 – 1162.
[12] Z. Hu, B. J. Deibert, J. Li, *Chem. Soc. Rev.* **2014**, *43*, 5815 – 5840.
[13] W. P. Lustig, J. Li, *Coord. Chem. Rev.* **2018**, *373*, 116 – 147.
[14] X.-Y. Liu, W. P. Lustig, J. Li, *ACS Energy Lett.* **2020**, *5*, 2671 – 2680.
[15] X. Li, J. Yu, D. J. Gosztola, H. C. Fry, P. Deria, *J. Am. Chem. Soc.* **2019**, *141*, 16849 – 16857.
[16] C. Y. Lee, O. K. Farha, B. J. Hong, A. A. Sarjeant, S. T. Nguyen, J. T. Hupp, *J. Am. Chem. Soc.* **2011**, *133*, 15858 – 15861.
[17] H.-J. Son, S. Jin, S. Patwardhan, S. J. Wezenberg, N. C. Jeong, M. So, C. E. Wilmer, A. A. Sarjeant, G. C. Schatz, R. Q. Snurr, O. K. Farha, G. P. Wiederrecht, J. T. Hupp, *J. Am. Chem. Soc.* **2013**, *135*, 862 – 869.
[18] D. E. Williams, J. A. Rietman, J. M. Maier, R. Tan, A. B. Greytak, M. D. Smith, J. A. Krause, N. B. Shustova, *J. Am. Chem. Soc.* **2014**, *136*, 11886 – 11889.
[19] E. A. Dolgopolova, D. E. Williams, A. B. Greytak, A. M. Rice, M. D. Smith, J. A. Krause, N. B. Shustova, *Angew. Chem. Int. Ed.* **2015**, *54*, 13639 – 13643; *Angew. Chem.* **2015**, *127*, 13843 – 13847.
[20] W. Danowski, F. Castiglioni, A. S. Sardjan, S. Krause, L. Pfeifer, D. Roke, A. Comotti, W. R. Browne, B. L. Feringa, *J. Am. Chem. Soc.* **2020**, *142*, 9048 – 9056.
[21] A. M. Rice, W. B. Fellows, E. A. Dolgopolova, A. B. Greytak, A. K. Vannucci, M. D. Smith, S. G. Karakalos, J. A. Krause, S. M. Avdoshenko, A. A. Popov, N. B. Shustova, *Angew. Chem. Int. Ed.* **2017**, *56*, 4525 – 4529; *Angew. Chem.* **2017**, *129*, 4596 – 4600.
[22] K. C. Park, C. Seo, G. Gupta, J. Kim, C. Y. Lee, *ACS Appl. Mater. Interfaces* **2017**, *9*, 38670 – 38677.
[23] A. Chakraborty, S. Ilic, M. Cai, B. J. Gibbons, X. Yang, C. C. Slamowitz, A. J. Morris, *J. Am. Chem. Soc.* **2020**, *142*, 20434 – 20443.
[24] J. Jia, L. Gutiérrez-Arzaluz, O. Shekhah, N. Alsadun, J. Czaban-Jóźwiak, S. Zhou, O. M. Bakr, O. F. Mohammed, M. Eddaoudi, *J. Am. Chem. Soc.* **2020**, *142*, 8580 – 8584.
[25] S. Yuan, W. Lu, Y. P. Chen, Q. Zhang, T. F. Liu, D. Feng, X. Wang, J. Qin, H. C. Zhou, *J. Am. Chem. Soc.* **2015**, *137*, 3177 – 3180.
[26] S. Yuan, Y. P. Chen, J. S. Qin, W. Lu, L. Zou, Q. Zhang, X. Wang, X. Sun, H. C. Zhou, *J. Am. Chem. Soc.* **2016**, *138*, 8912 – 8919.
[27] E. A. Dolgopolova, O. A. Ejegbavwo, C. R. Martin, M. D. Smith, W. Setyawan, S. G. Karakalos, C. H. Henager, H.-C. zur Loye, N. B. Shustova, *J. Am. Chem. Soc.* **2017**, *139*, 16852 – 16861.
[28] X. Zhang, B. L. Frey, Y. S. Chen, J. Zhang, *J. Am. Chem. Soc.* **2018**, *140*, 7710 – 7715.
[29] O. A. Ejegbavwo, C. R. Martin, O. A. Olorunfemi, G. A. Leith, R. T. Ly, A. M. Rice, E. A. Dolgopolova, M. D. Smith, S. G. Karakalos, N. Birkner, B. A. Powell, S. Pandey, R. J. Koch, S. T. Misture, H.-C. zur Loye, S. R. Phillpot, K. S. Brinkman, N. B. Shustova, *J. Am. Chem. Soc.* **2019**, *141*, 11628 – 11640.
[30] A. A. Berseneva, C. R. Martin, V. A. Galitskiy, O. A. Ejegbavwo, G. A. Leith, R. T. Ly, A. M. Rice, E. A. Dolgopolova, M. D. Smith, H. C. zur Loye, D. P. DiPrete, J. W. Amoroso, N. B. Shustova, *Inorg. Chem.* **2020**, *59*, 179 – 183.
[31] J. Pang, S. Yuan, J. S. Qin, C. T. Lollar, N. Huang, J. Li, Q. Wang, M. Wu, D. Yuan, M. Hong, H. C. Zhou, *J. Am. Chem. Soc.* **2019**, *141*, 3129 – 3136.
[32] J. Pang, Z. Di, J. S. Qin, S. Yuan, C. T. Lollar, J. Li, P. Zhang, M. Wu, D. Yuan, M. Hong, H. C. Zhou, *J. Am. Chem. Soc.* **2020**, *142*, 15020 – 15026.
[33] J. Li, S. Yuan, J.-S. Qin, J. Pang, P. Zhang, Y. Zhang, Y. Huang, H. F. Drake, W. R. Liu, H.-C. Zhou, *Angew. Chem. Int. Ed.* **2020**, *59*, 9319 – 9323; *Angew. Chem.* **2020**, *132*, 9405 – 9409.
[34] C. X. Chen, Z. Wei, J. J. Jiang, Y. Z. Fan, S. P. Zheng, C. C. Cao, Y. H. Li, D. Fenske, C. Y. Su, *Angew. Chem. Int. Ed.* **2016**, *55*, 9932 – 9936; *Angew. Chem.* **2016**, *128*, 10086 – 10090.
[35] C. X. Chen, Z. W. Wei, J. J. Jiang, S. P. Zheng, H. P. Wang, Q. F. Qiu, C. C. Cao, D. Fenske, C. Y. Su, *J. Am. Chem. Soc.* **2017**, *139*, 6034 – 6037.
[36] S. Wu, D. Ren, K. Zhou, H.-L. Xia, X.-Y. Liu, X. Wang, J. Li, *J. Am. Chem. Soc.* **2021**, *143*, 10547 – 10552.
[37] L. Chen, L. Wang, X. Jing, F. Wang, *J. Mater. Chem.* **2011**, *21*, 10265 – 10267.
[38] S. Benson, A. Fernandez, N. D. Barth, F. de Moliner, M. H. Horrocks, C. S. Herrington, J. L. Abad, A. Delgado, L. Kelly, Z. Chang, Y. Feng, M. Nishiura, Y. Hori, K. Kikuchi, M. Vendrell, *Angew. Chem. Int. Ed.* **2019**, *58*, 6911 – 6915; *Angew. Chem.* **2019**, *131*, 6985 – 6989.
[39] M. A. Nasalevich, C. H. Hendon, J. G. Santaclara, K. Svane, B. van der Linden, S. L. Veber, M. V. Fedin, A. J. Houtepen, M. A. van der Veen, F. Kapteijn, A. Walsh, J. Gascon, *Sci. Rep.* **2016**, *6*, 23676.
[40] J. Yu, J. Park, A. Van Wyk, G. Rumbles, P. Deria, *J. Am. Chem. Soc.* **2018**, *140*, 10488 – 10496.
[41] J. Yu, X. Li, P. Deria, *ACS Sustainable Chem. Eng.* **2019**, *7*, 1841 – 1854.

Manuscript received: August 5, 2021
Accepted manuscript online: September 17, 2021
Version of record online: October 18, 2021

